Sulfur's impact on core evolution and magnetic field generation on Ganymede

Steven A. Hauck, II,[1] Jonathan M. Aurnou ,[2] and Andrew J. Dombard [3]

[1]   Analysis of the melting relationships of potential core forming materials in Ganymede indicate that fluid motions, a requirement for a dynamo origin for the satellite's magnetic field, may be driven, in part, either by iron (Fe) "snow" forming below the core-mantle boundary or solid iron sulfide (FeS) floating upward from the deep core. Eutectic melting temperatures and eutectic sulfur contents in the binary Fe-FeS system decrease with increasing pressure within the interval of core pressures on Ganymede (<14 GPa). Comparison of melting temperatures to adiabatic temperature gradients in the core suggests that solid iron is thermodynamically stable at shallow levels for bulk core compositions more iron-rich than eutectic (i.e., <21 wt % S). Calculations based on high-pressure solid-liquid phase relationships in the Fe-FeS system indicate that iron snow or floatation of solid iron sulfide, depending on whether the core composition is more or less iron-rich than eutectic, is an inevitable consequence of cooling Ganymede's core. These results are robust over a wide range of plausible three-layer internal structures and thermal evolution scenarios. For precipitation regimes that include Fe-snow, we present scaling arguments that give typical Rossby and magnetic Reynolds numbers consistent with dynamo action occurring in Ganymede's core. Furthermore, by applying recently derived scaling relationships relating magnetic field strength to buoyancy flux, we obtain estimates of surface magnetic field strength comparable with observed values.

1.   Introduction

[2]   Flybys of Ganymede, Jupiter's largest moon, by NASA's Galileo spacecraft provided the most detailed view to date of its internal structure and dynamics [e.g., *Anderson et al.*, 1996; *Kivelson et al.*, 1996; *Schubert et al.*, 1996; *Palguta et al.*, 2006]. Ganymede is the most centrally concentrated, largely solid body known in the solar system as indicated by the nondimensional polar moment of inertia (C/MR^2) of 0.3115 [*Schubert et al.*, 2004]. On the basis of this moment of inertia and Ganymede's bulk density, a three-layer model (ice, rock, and metal) appears to be the most consistent with observations [*Anderson et al.*, 1996; *Schubert et al.*, 1996], implying complete differentiation. One of the best corroborating clues as to the nature of Ganymede's interior comes from the surprising detection of its intrinsic magnetic field with a permanent dipole moment that has an equatorial field magnitude of >700 nT and that stands off the Jovian magnetic field [*Kivelson et al.*, 1996,

2002]. The existence of a magnetic field suggests that either there is a layer with significant remanent magnetization [e.g., *Crary and Bagenal*, 1998] or the field is generated by convection in an electrically conducting fluid, likely a liquid portion of a metallic core [*Schubert et al.*, 1996; *Kivelson et al.*, 2002].

[3]   An active dynamo within Ganymede's core is the preferred interpretation of Galileo magnetic field measurements [*Schubert et al.*, 1996; *Kivelson et al.*, 2002], which places Jupiter's largest moon in a unique category. It is the only known satellite in the solar system with an intrinsic global magnetic field and is one of only three solid bodies known with one at present (i.e., also Earth and Mercury, though Mars likely had a global field in the past). The existence of a hydromagnetic dynamo requires motions within an electrically conducting fluid [e.g., *Gubbins and Roberts*, 1987; *Merrill et al.*, 1998]. In the case of Ganymede, this implies that (1) the metallic core is at least partially molten because motions in an electrically conductive, salty ocean would have to be several orders of magnitude stronger than reasonable predictions suggest [*Schubert et al.*, 1996], and (2) there is a process responsible for driving motions in that molten core. Here we assume that these motions are due to buoyancy-driven convection. Possible thermal buoyancy sources for convection are cooling by the mantle, release of gravitational and latent heat due to inner core solidification, and volumetric heating from the decay of ^{40}K [e.g., *Merrill et al.*, 1998]. Possible

---

[1]Department of Geological Sciences, Case Western Reserve University, Cleveland, Ohio, USA.
[2]Department of Earth and Space Sciences, University of California at Los Angeles, Los Angeles, California, USA.
[3]Applied Physics Laboratory, Johns Hopkins University, Laurel, Maryland, USA.

compositional sources of buoyancy include the expulsion of light constituents upon freezing of relatively pure iron and the settling or floatation of solid precipitates. A compositional source is the most robust of these mechanisms because a thermally driven dynamo is subject to the inherent inefficiencies of a heat engine [e.g., *Gubbins*, 1977; *Loper*, 1978; *Loper and Roberts*, 1979, 1983].

[4] A candidate for the dominant core-forming assemblage is an alloy of iron (Fe) and sulfur (S), as has been proposed for the core of the Earth [e.g., *Murthy and Hall*, 1970]. A highly siderophile element, sulfur also had a high availability in the proto-solar system [*Hillgren et al.*, 2000]; these ideas coupled with the composition of CI chondrites [*McKinnon*, 1996; *Schubert et al.*, 2004] and recent high-pressure hydrothermal experiments on potential Ganymede-forming materials [*Scott et al.*, 2002] indicate that sulfur may be an important constituent of Ganymede's core. On the other hand, the unknown oxidation state of the interior during differentiation limits the ability to constrain whether the composition of a sulfur-bearing core is on the Fe- or FeS-rich side of the eutectic composition [e.g., *Scott et al.*, 2002].

[5] Incorporation of sulfur into a metallic core has two major effects: reduction in bulk density and a strong melting-point depression [e.g., *Usselman*, 1975; *Fei et al.*, 1997]. Experiments in the last decade have demonstrated that at pressures less than ~14 GPa the eutectic melting temperature in the iron – iron sulfide (Fe-FeS) system decreases with increasing pressure [*Fei et al.*, 1995, 1997, 2000], opposite the behavior of alloys at Earth's core pressures [*Boehler*, 1992, 1996; *Anderson*, 2003]. While this fact has not gone unrecognized with respect to Ganymede [*Kuang and Stevenson*, 1996; *McKinnon*, 1996], the potentially profound implications for the satellite's evolution and generation of its magnetic field are not well understood.

[6] Given the unconstrained composition of Ganymede's core, convection driven by compositional buoyancy could proceed in several ways [*McKinnon*, 1996]. First, at low sulfur contents, nominally pure, solid Fe might precipitate to form an inner core and expel the lighter constituent, which would rise within the outer core. Second, for a sulfur-rich composition, solid FeS might precipitate deep within the core, buoyantly rise, and remelt at higher levels. Alternatively, because of the decrease in eutectic temperature in the Fe-FeS system with increasing pressure (i.e., increasing depth) [*Fei et al.*, 1997, 2000], solids might snow down from the core-mantle boundary at compositions with subeutectic sulfur content, only to remelt at deeper levels. The latter two mechanisms are examples of relatively unique ways of driving core convection that may have distinct implications for the evolution of Ganymede's core.

[7] The results from the Galileo spacecraft indicate that Ganymede has a highly differentiated interior and a magnetic field of internal origin [*Anderson et al.*, 1996; *Kivelson et al.*, 1996; *Schubert et al.*, 1996]. These observations, coupled with the fact that pressures in the satellite's core (<14 GPa) overlap with those in laboratory experiments on potential core-forming materials [*Fei et al.*, 1997; 2000], provide a unique opportunity to study compositional buoyancy driven mechanisms of magnetic field generation. We attempt to understand the conditions, especially core com-

position, that are conducive to the present-day generation of Ganymede's magnetic field and to elucidate the mechanisms by which the core may have evolved. We focus on the relevant processes rather than developing a definitive history for Ganymede; hence a set of simplified, demonstrative models, rather than exhaustive ones, is presented. Finally, we discuss the implications for Ganymede's internal structure and magnetic field generation.

2. Approach

[8] The implications of the complex melting behavior of Fe-FeS alloys at pressures <14 GPa for core evolution and potential magnetic field generation are investigated for a body like Ganymede. The approach is to (1) calculate a suite of internal structure models to determine the thickness of the ice, mantle, and core layers as well as the pressures in the core, (2) determine the solid-liquid phase stability and composition as a function of radius in the core and temperature, and (3) model core evolution as a function of core composition, levels of mantle radioactive heat production, and satellite internal structure.

2.1. Internal Structure

[9] We calculate a suite of three-layer, internal structure models that are consistent with Ganymede's moment-of-inertia factor (MOI), $I/MR^2 = C/MR^2 - (2/3) J_2 \approx C/MR^2 \approx 0.3115$ (because $J_2 \sim 10^{-4}$), and bulk density (~1942 kg/m^3) [*Schubert et al.*, 2004]. The densities of the ice and rock mantle layers are assumed to be constant and are unconstrained; therefore a range of values is investigated. In contrast, the density structure of the core is allowed to vary radially and is assumed to be well characterized by a third-order Birch-Murnaghan equation of state [e.g., *Poirier*, 2000] that accounts for the pressure and temperature dependence of the density:

$$P = \frac{3K_0}{2}\left[\left(\frac{\rho}{\rho_0}\right)^{7/3} - \left(\frac{\rho}{\rho_0}\right)^{5/3}\right] \times \left[1 + \frac{3}{4}\left(K_0' - 4\right)\left\{\left(\frac{\rho}{\rho_0}\right)^{2/3} - 1\right\}\right] + \alpha_0 K_0 (T - 298), \quad (1)$$

where pressure (P) is a function of density (ρ), standard-state density (ρ_0), isothermal bulk modulus (K_0), the derivative of the bulk modulus with respect to pressure (K_0'), volumetric thermal expansivity (α_0), and temperature (T).

[10] A forward model, grid-search approach is employed to calculate solutions to the equations of hydrostatic equilibrium for a spherically symmetric body [e.g., *Turcotte and Schubert*, 1982] that satisfy the observed bulk density and MOI. For an individual model, the densities and thicknesses of the ice and rock layers are specified, as is the radius and bulk sulfur content of the core. Bulk properties of the core are estimated by interpolating between Fe and FeS parameters as a function of bulk sulfur content. We employ parameters for Fe-FeS liquids where available [e.g., *Anderson and Ahrens*, 1994; *Sanloup et al.*, 2000; *Balog et al.*, 2003]; interpolations are linear between end-members as a function of bulk sulfur content (end-members for molecular weight and molecular volume are used for calculating ρ_0) with the exception of the bulk modulus (K_0). For bulk

Table 1. Structural Model Parameters

Parameter	Symbol	Value	Units
Normalized moment of inertia	C/MR_p^2	0.3115	-
Bulk density of satellite	$\bar{\rho}$	1942	kg/m³
Radius of satellite	R_p	2631	m
Ice density	ρ_i	1000–1300	kg/m³
Mantle density	ρ_m	2800–3600	kg/m³
Liquid Fe density	$\rho_{0,\ Fe}$	7020	kg/m³
Liquid FeS density	$\rho_{0,\ FeS}$	5333	kg/m³
Bulk modulus coefficient	K_{0a}	5.54×10^{11}	Pa
Bulk modulus coefficient	K_{0b}	3.91×10^{11}	Pa
Bulk modulus coefficient	K_{0c}	8.13×10^{10}	Pa
Pressured derivative of K_0	$K'_{0,\ Fe}$	4.6	-
Pressured derivative of K_0	$K'_{0,\ FeS}$	5.0	-
Thermal expansivity	$\alpha_{0,\ Fe}$	9.2×10^{-5}	K⁻¹
Thermal expansivity	$\alpha_{0,\ FeS}$	1.1×10^{-4}	K⁻¹

modulus we implement a quadratic fit ($K_0 = K_{0a}\chi_S^2 + K_{0b}\chi_S + K_{0c}$) of the data from *Sanloup et al.* [2000] as a function of sulfur mass fraction, χ_S. An iterative procedure is used to calculate the density structure in the core based upon equation (1). Models that match bulk density and the MOI within 0.01% are considered viable. The larger, formal uncertainties on the observed parameters are neglected because a wide range of structures is considered, and we do not attempt to find best fit structures, only to utilize reasonable structures as input for further modeling. The parameters employed are listed in Table 1. Figure 1 illustrates a range of possible models consistent with observations for an assumed bulk core sulfur content of 10 wt %. Higher densities for the surface ice layer translate into thinner layers of ice. Furthermore, for a given mantle density, an increase in ice layer density trades-off with an increase in the fraction size of the metallic core; for ice densities less than 1300 kg m⁻³ and rock mantle densities greater than 2800 kg m⁻³, the core occupies less than 45% of Ganymede's radius, which amounts to less than ~10% of the moon's total volume.

2.2. Solid Precipitation

[11] Precipitation of solid iron to form the Earth's inner core is a dominant dynamical process that likely contributes significantly to the generation of our planet's magnetic field [e.g., *Buffett et al.*, 1996; *Merrill et al.*, 1998]. Similar processes are plausibly important for Ganymede's internal magnetic field; however, the melting relationships for core alloys at lower pressures (e.g., the ~6–10 GPa range for Ganymede's core) differ from those at higher pressure, especially for the Fe-FeS system [*Fei et al.*, 1997, 2000]. Contrary to the situation of the Earth, however, eutectic melting temperatures decrease with increasing pressure up to ~14 GPa, as do eutectic composition sulfur contents at pressures up to ~7 GPa, in the Fe-FeS system [*Fei et al.*, 1997, 2000]. This implies that shallow precipitation of Fe (i.e., near the core-mantle boundary) may be preferred relative to deep precipitation (i.e., at the inner core – outer core boundary) [*Kuang and Stevenson*, 1996; *McKinnon*, 1996; *Hauck et al.*, 2002].

[12] In a binary system, knowledge of the local values of pressure, temperature, and composition, and the dependence of the melting curve on these parameters, results in unique knowledge of the phases present everywhere in the system. These conditions are met within our model core system. For example, by assuming an initial compositionally homoge-

neous system with a known radial pressure distribution and an assumed adiabatic temperature distribution, the phases are calculable via two well-known, fundamental rules for equilibrium phase diagrams [e.g., *Brownlow*, 1996]: (1) the phase rule, which describes the degrees of freedom in the thermodynamic system, and (2) the lever rule, which provides for calculation of the relative amounts of solid and liquid phases and the solid and liquid compositions for a given temperature and bulk composition. This state describes thermodynamic equilibrium, but not necessarily fluid mechanical equilibrium. In the case of shallow Fe precipitation, which occurs at compositions more Fe-rich than eutectic, solid-Fe is thermodynamically stable near the core-mantle boundary (CMB), but the dense precipitate is buoyantly unstable and will tend to fall under gravity toward the center of the core. Thus the compositional state at any radial position (depth) will change due to the compositional advection of the falling precipitates. Near the CMB, the adiabat and the liquidus will be colinear due to the fact that the lever rule requires that the residual liquid have the liquidus composition at a given temperature (provided by the adiabat) and because dense, solid iron will be hydrodynamically unstable and will fall inward, leaving behind a liquid with the composition of the liquidus for the local temperature and pressure. Vigorous convection will be unable to compositionally homogenize the system because any liquid iron mixed upward from deeper levels would be thermodynamically unstable and precipitate as a Fe-snow again; with our assumptions that precipitation is neither kinetically, nor nucleation, inhibited this process will be immediate. Deeper within the core, the composition will become more Fe rich because of the accumulation of the Fe that falls inward as a solid and subsequently remelts;
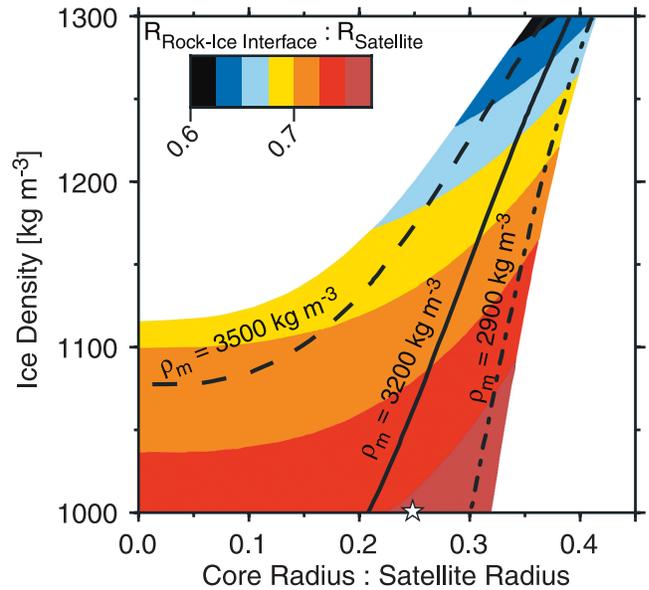

Figure 1. Three-layer internal structures that satisfy Ganymede's bulk density and moment of inertia for a model with a liquid core containing 10 wt % S. Shaded contours indicate location of rock-ice interface as a function of ice layer density and core radius. Contours of rock-mantle density are indicated. The white star indicates the location of parameters employed in Figure 4.
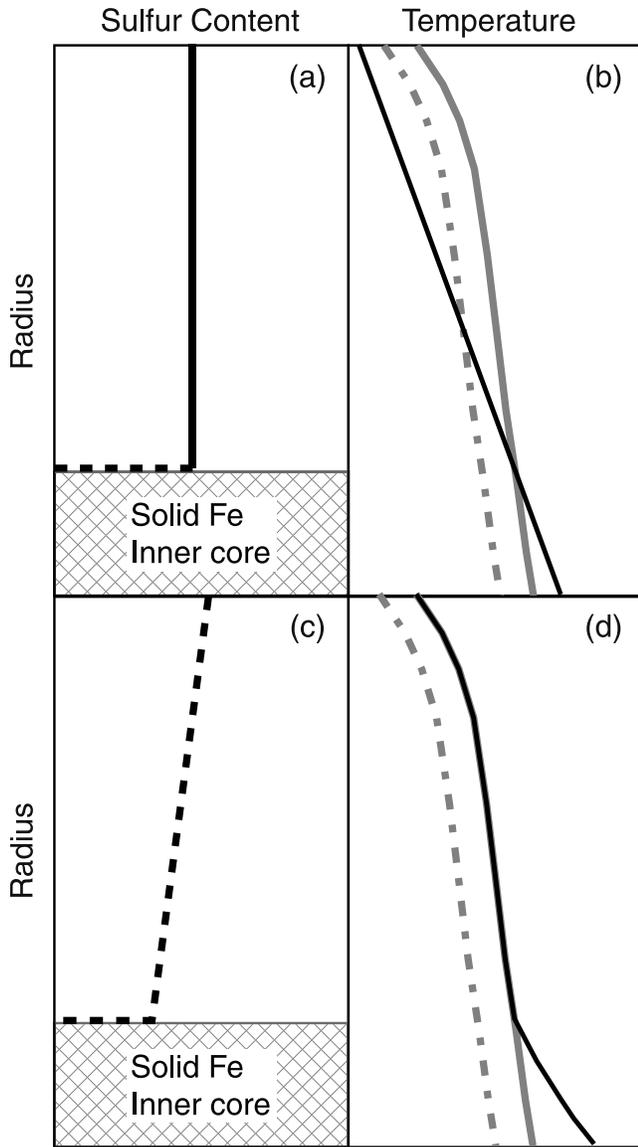
Figure 2. Schematic diagram of two potential modes of solid iron precipitation in Ganymede's core. (a,c) radial variation in composition. The hatched areas are the pure solid iron inner core, the thick black lines show the variation in sulfur content, dashed segments indicate that precipitation of solid would be thermodynamically favored at these locations with additional cooling. (b,d) the radial adiabatic and melting temperature variation. The thick gray lines are the core temperatures, solid line is consistent with compositional panel to the left, the dash-dot line indicates an increment of cooling. The black line indicates the melting temperature. Figures 2a and 2b indicate an Earth-like case where the (Figure 2a) composition of the outer core is relatively homogeneous and all solid Fe precipitation occurs at the ICB. Melting temperatures (Figure 2b) are less than the actual temperatures in the outer core, an increment of cooling results in growth of the inner core and an increase in the sulfur content of the outer core by mass balance. Figures 2c and 2d indicate a case where melting temperatures for a constant bulk composition would decrease with depth.

ultimately the sequestration of iron-rich material deep in the core, with its concomitant relatively higher melting temperature, leads to growth of a solid iron inner core upon which shallowly formed Fe-snow precipitates. Two examples of this process are schematically illustrated in Figure 2, which plots the radial variation in sulfur content (Figures 2a and 2c) and core and melting temperatures (Figures 2b and 2d). Phase stability is determined by comparison of the local temperature (gray lines in Figures 2b and 2d) to the melting temperature of a core alloy (black lines); a local temperature below the melting temperature implies precipitation of solid. An Earth-like example is illustrated in Figures 2a and 2b, which indicates precipitation of solid Fe at the inner core – outer core boundary (ICB), and melting temperatures above the ICB are less than the temperature in the outer core. A mode in which precipitation of solid Fe is thermodynamically favored throughout the outer core is shown in Figures 2c and 2d, illustrating that the melting and adiabatic core temperatures are colinear, which is due to the inward migration of solids and consequent change in local composition.

[13] In order to assess the potential dynamical implications of precipitation of solids within Ganymede's core, we calculate the solid-liquid phase stability as a function of temperature and radial position within the core as well as the potential accumulation of solids and resulting changes in local composition. Sulfur is assumed to be essentially insoluble in solid Fe and hence resides solely in the liquid phase at temperatures above eutectic; therefore the melting temperature depends directly on the local sulfur content. Specification of the core-mantle boundary temperature and assumption of an adiabatic outer core fully constrains temperatures. The adiabatic temperature profile is given by

$$T = T_{cmb} \exp\left[\frac{\alpha(P(r) - P_{cmb})}{\rho_c c_c}\right], \qquad (2)$$

where T_{cmb} is the core-mantle boundary temperature, α is thermal expansivity, $P(r)$ and P_{cmb} are the pressures as a function of radial position and at the core-mantle boundary respectively, ρ_c is the density of the core, and c_c is the specific heat. Core pressures are related to the core density, radially varying gravity, and radial position where we assume that local core gravity varies as $g(r) = g_{cmb}r/R_{cmb}$ [e.g., *Stevenson et al.*, 1983]. Though more complicated formulations for the adiabatic temperature profile that include the effect of the pressure dependence of α do exist [e.g., *Labrosse et al.*, 2001], this formulation is sufficiently accurate to second-order [*Labrosse*, 2003].

[14] We apply a simplified melting curve based on the Fe-FeS system [*Fei et al.*, 1997, 2000]. The melting temperature is given using the simplified form [*Stevenson et al.*, 1983]

$$T_m = T_{m0,(\text{Fe,FeS})}\left[1 + T_{m1,(\text{Fe,FeS})}P + T_{m2,(\text{Fe,FeS})}P^2\right]\left[1 - \alpha_c \chi_s\right]. \qquad (3)$$

The preceding terms with a subscripted (Fe,FeS) represent quadratic coefficients for end-member melting temperatures. The choice of which coefficient is employed depends

Table 2. Core Melting Parameters

Symbol	Value	Units
$T_{m0,\ Fe}$	1809	K
$T_{m1,\ Fe}$	1.99×10^{-11}	Pa^{-1}
$T_{m2,\ Fe}$	-1.84×10^{-22}	Pa^{-2}
$T_{m0,\ FeS}$	1495	K
$T_{m1,\ FeS}$	1.97×10^{-11}	Pa^{-1}
$T_{m2,\ FeS}$	-1.43×10^{-22}	Pa^{-2}
T_{eu0}	1261	K
T_{eu1}	-6.91×10^{-12}	Pa^{-1}
$\chi_{eu0,\ <7\ GPa}$	0.31	-
$\chi_{eu1,\ <7\ GPa}$	-4.74×10^{-2}	Pa^{-1}
$\chi_{eu0,\ >7\ GPa}$	0.207	-
$\chi_{eu1,\ >7\ GPa}$	0	-

on whether the alloy composition is more Fe- or FeS-rich as compared to the eutectic composition. The terms in the last set of brackets (α_c slope of the liquidus, χ_s the mass fraction of sulfur) define the melting point depression due to the inclusion of a light element, sulfur in this case. Though a standard practice [e.g., *Stevenson et al.*, 1983; *Schubert et al.*, 1988; *Hauck et al.*, 2004], the linear liquidus curve as a function of alloying element content generally underestimates the melting temperature between the pure end-member and eutectic compositions, which are better known [e.g., *Boehler*, 1992, 1996; *Anderson*, 2003]. However, this simplification is acceptable given the dearth of available data for the high-pressure melting temperatures of Fe-FeS compounds as a function of sulfur content and that our goal is to demonstrate a process, not develop a definitive internal model for Ganymede. The liquidus slope as a function of
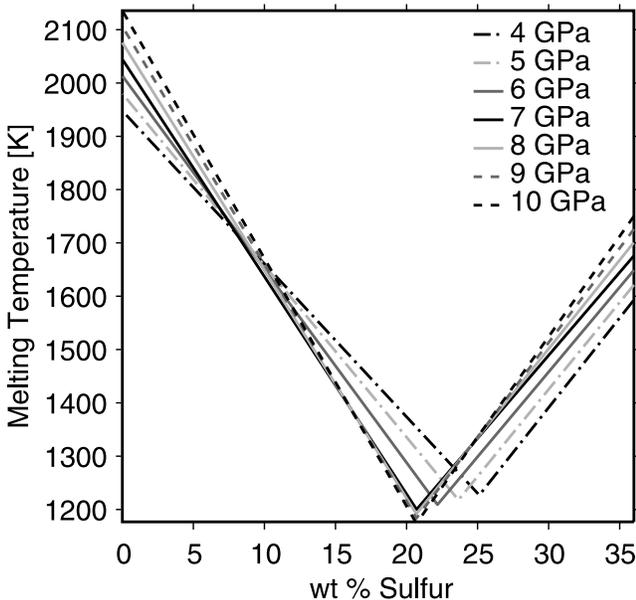
composition, α_c, is determined from available data for the Fe-FeS system [*Fei et al.*, 1997, 2000] by the following equation, with the parameters listed in Table 2:

$$\alpha_c = \frac{T_{m0,(Fe,FeS)}\left[1 + T_{m1,(Fe,FeS)}P + T_{m2,(Fe,FeS)}P^2\right] - T_{eu0}[1 + T_{eu1}P]}{T_{m0,(Fe,FeS)}\chi_{eu0}[1 + \chi_{eu1}P]}.$$

(4)

The slope of the liquidus is a function of the end-member (Fe or FeS) melting temperature, the eutectic temperature (T_{eu0} and T_{eu1} coefficients), the eutectic composition (χ_{eu0} and χ_{eu1} coefficients), and pressure. Figure 3 illustrates the model Fe-FeS melting system described by equations (3) and (4). The melting temperatures plotted in Figure 3 clearly indicate both the decreasing eutectic melting temperatures and eutectic sulfur contents (the latter only up to 7 GPa) as a function of increasing pressure.

2.3. Thermal Evolution

[15] We model the evolution of Ganymede's deep interior using a parameterized mantle convection technique [e.g., *Stevenson et al.*, 1983] modified from the typical implementation to include the potential transition from convective to fully conductive heat loss [*Hauck et al.*, 2004], and we explicitly solve the nonlinear, time-dependent, heat conduction equation in the thermal lithosphere via a finite element solution with adaptive remeshing [*Hauck and Phillips*, 2002]. Basic model parameters are listed in Table 3. A one-dimensional representation of convective heat transfer in spherical shells (i.e., metallic core, rock mantle) is employed to calculate possible thermal evolutions. Solution of the basic relationship for conservation of thermal energy in the rock mantle is parameterized via a relationship between the vigor of convection (described by the Rayleigh number, Ra, the ratio of buoyancy to viscous forces) and the efficiency of convective heat transfer (defined by the Nusselt number, Nu, the ratio of the total heat flux to the conducted heat flux) [e.g., *Schubert et al.*, 2001]. Rock mantles tend to behave like fluids with strongly temperature-dependent viscosities, which operate in the stagnant-lid regime when viscosity contrasts are large [*Solomatov*, 1995]. In this stagnant-lid regime, we use $Nu = (0.31 + 0.22n)\theta^{\frac{-2(n+1)}{(n+2)}} Ra_i^{\frac{n}{n+2}}$ [*Solomatov and Moresi*, 2000], where n is the exponent of the deviatoric stress in the flow law (e.g., $n=1$ for Newtonian fluids), and θ is the natural logarithm of the viscosity contrast across the layer. While

Figure 3. Model melting temperatures as a function of bulk core sulfur content in the Fe-FeS for pressures from 4 to 10 GPa. Melting temperatures of pure Fe, pure FeS, and eutectic compositions match available data from the literature [*Boehler*, 1992; *Fei et al.*, 1995; *Boehler*, 1996; *Fei et al.*, 1997, 2000; *Anderson*, 2003]; temperatures are the result of linear interpolation between pure end-members and eutectic values at intermediate compositions.

Table 3. Model Parameters

Parameter	Symbol	Value	Units
Heat capacity of mantle	c_m	1149	J/(kg K)
Heat capacity of core	c_c	800	J/(kg K)
Ice-rock interface temperature	T_s	275	K
Initial mantle temperature	T_{u0}	1800	K
Initial CMB temperature	T_{c0}	2000	K
Mantle thermal expansivity	α_v	3×10^{-5}	K^{-1}
Mantle thermal diffusivity	κ	1×10^{-6}	m^2/s
Mantle thermal conductivity	k	4	W/(m K)
Ductile creep viscosity constant	A^*	2×10^{18}	1/s
Rigidity of mantle	μ	8×10^{10}	Pa
Ductile creep stress exponent	n	3	-
Ductile creep activation energy	E_a	4.3×10^5	J/mol
Ductile creep activation volume	V	1.5×10^{-5}	m^3/mol
Iron heat of fusion	L	2.5×10^5	J/kg

we do not a priori rule out that some sort of lithospheric recycling has occurred on Ganymede, this analysis focuses solely on stagnant-lid mantle convection. This approach allows us to concentrate the present study on the effects of sulfur composition on core evolution and magnetic field generation.

[16] The model of Ganymede's thermal evolution involves solving the conservation of energy equation as a function of time

$$\frac{4}{3}\pi\left(R_m^3 - R_c^3\right)\left[H - \rho_m c_m \frac{d\langle T_m\rangle}{dt}\right] = 4\pi\left(q_s R_m^2 - q_c R_c^2\right), \quad (5)$$

where the time rate of change of heat in the rock mantle is equal to the difference of the heat lost at the rock surface and input at the CMB as a function of the radius of the rock-ice interface and of the CMB, R_m and R_c respectively, radiogenic heat generation, H, average mantle temperature T_m, mantle density, ρ_m, heat capacity, c_m, and the rock-ice interface and core heat fluxes, q_s, and q_c. The solution is parameterized via the *Ra-Nu* relationship that relates mantle temperatures to heat loss for a convecting mantle with internal heating, a cooling (and possibly solidifying) core, and a growing mantle lithosphere. Core cooling, the latent heat of freezing, and the gravitational energy released upon inner core growth follows equations (3)–(7) of *Stevenson et al.* [1983], though we utilize the Fe-FeS melting relationships previously described and an expression for the gravitational energy release as a function of bulk core sulfur content and the relative size of the inner core [*Schubert et al.*, 1988, equation (13)]. Convection within the ice layer is not modeled, instead the ice-silicate interface is assumed to be isothermal. Transfer of heat through the high viscosity rock mantle is the bottleneck to heat loss, not the lower viscosity icy layer, which argues that for the purposes of investigating processes in the core, this is a reasonable assumption.

[17] The abundance of heat-producing elements is also unconstrained, but a CI chondritic composition may be a reasonable starting assumption. We also investigate the effects of heat-production compositions that are one half and twice the CI chondritic concentrations of U, Th, and K in order to investigate a plausible range. Recent structural models using equations of state and physical properties of likely icy satellite constituents as potential constraints suggest that a bulk composition similar to L or LL chondrites may be representative of Ganymede's non-ice interior [*Kuskov and Kronrod*, 2001]; such a composition fits within our range. As the timing of differentiation or any tidal heating due to passage through and capture into resonances [*Showman et al.*, 1997] is uncertain, our initial models start with a fully differentiated planet at ~4.5 Ga [*Kirk and Stevenson*, 1987]; yet we recognize that this state may have been reached at a more recent epoch. We assume that the viscosity of the silicate layer can be approximated by that of a wet, non-Newtonian, pressure- and temperature-dependent, olivine rheology [*Karato and Wu*, 1993]:

$$\eta = \frac{\mu^n}{3^{(n+1)/2}A^*}\left(\frac{1}{\sigma}\right)^{n-1}\exp\left(\frac{E+PV}{R_{gas}T}\right). \quad (6)$$

Equation (6) describes the implemented power law constitutive relationship for viscosity, which depends on rigidity (μ), and an experimentally determined constant, A^*, and exponentially on temperature, pressure, activation energy (E) and activation volume (V), and the gas constant (R_{gas}). Rock mantle viscosity is non-linear and depends on the driving stress (σ) with a power law exponent of n. The numerical prefactor is the necessary geometric proportionality factor that relates the equivalent stress measured in experiments with the driving stress of mantle convection [*Ranalli*, 1995]. Relevant model outputs include characteristic mantle and core-mantle boundary temperatures, heat fluxes, boundary layer thicknesses, as well as the location of the boundary between pure liquids and regions that may contain solid precipitates (e.g., the size of the inner core). Additional details of the implementation of the basic thermal evolution calculations are also described by *Hauck and Phillips* [2002] and *Hauck et al.* [2004].

3. Results

[18] On the basis of three-layer internal structure models similar to those presented in Figure 1, but with a wide range of bulk core sulfur contents, we calculate a suite of models of the thermal and physical state of Ganymede in order to understand the potential implications of the melting behavior of Fe-FeS alloys at modest pressures for the evolution and current state of the satellite's interior as well as generation of its magnetic field. In particular, we focus first on outlining the full-range of possible physical states for the core (e.g., all liquid, Fe-snow, etc.) as a function of temperature and composition. Then we apply this knowledge to parameterized models of Ganymede's evolution in order to understand which physical state(s) might be most relevant to the current state of the satellite.

3.1. Core States

[19] Using the results from the three-layer structural models we developed (e.g., Figure 1) as input, we calculate the phase and composition at 300 locations in the outer core as a function of temperature. Figure 4 illustrates the results of a typical model run where the composition of the core is indicated as a function of normalized core radius (R/R_c) and core-mantle boundary temperature. This model has a bulk core sulfur content of 10 wt %, R_c = 651 km, ρ_m = 3100 kg m^{-3}, ρ_i = 1000 kg m^{-3}, R_m = 1982 km, and pressures range from approximately 5.8–8.0 GPa in the core. At high temperatures, above the melting point of the 10 wt % S alloy, the entire core is molten. The first solids are stable at a $T_{cmb} \approx 1650$ K and form shallowly below the CMB. The short-dashed line in Figure 4a indicates the stability boundary, above the line Fe-snow can form, below the line only liquid is stable. However, because of the relatively higher density of the solid Fe-snow, as compared to the surrounding liquid, it falls deeper into the core where it remelts, which sets up the modest compositional stratification of decreasing sulfur content with depth. Thus the contour shading in Figure 4a indicates that the deeper portion of the core has less sulfur than the bulk sulfur content of 10 wt %. At CMB temperatures less than about 1635 K, Fe-snow is still stable at shallow levels, but the relatively higher Fe contents (and hence higher melting temperatures) deeper in
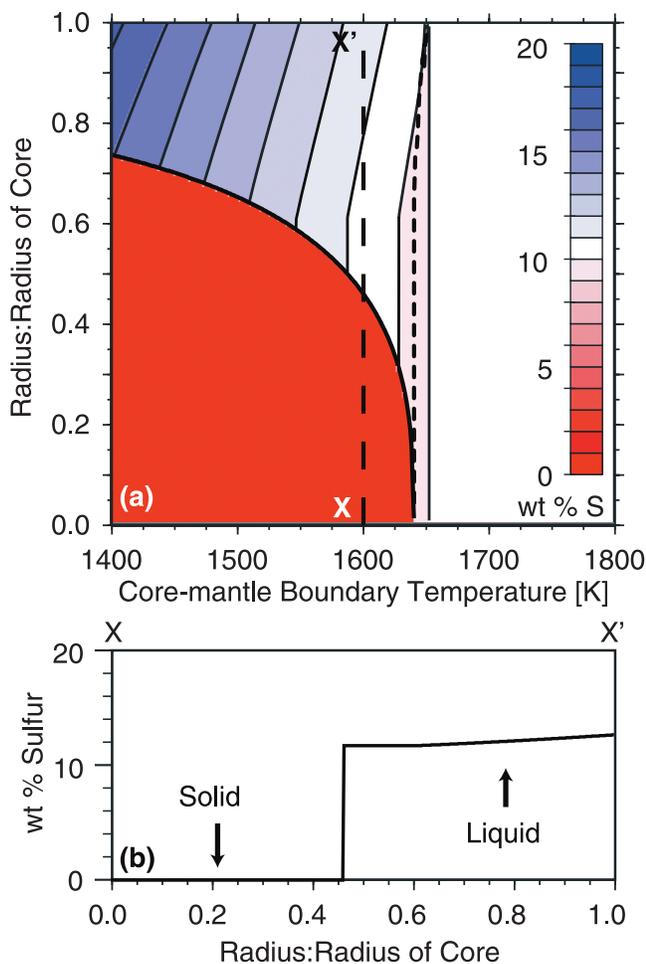
Figure 4. Example of physical state of the core for an initial core sulfur content of 10 wt %. (a) Local composition as a function of core-mantle boundary temperature. Shaded contours indicate local sulfur content due to Fe precipitation. Short-dashed line indicates boundary between the region where Fe-snow is possible and a deeper zone where only the liquid phase is stable (no inner core). The large red zone in the lower left is the inner core. Long-dashed line (X-X′) profile indicates location for (b) local composition as a function of radial position for a core-mantle boundary temperature of 1600 K.

the core lead to concurrent precipitation of solid Fe at the ICB (e.g., Figures 2c and 2d). This view of solid Fe precipitation in the core is broadly similar to the Earth with the exceptions that shallow precipitation of solid Fe is not predicted in the Earth nor is the consequent modest compositional stratification across the outer core. Figure 4b illustrates the variation in composition as a function of radial position in the core for a CMB temperature of 1600 K (along the long-dashed line from X-X′ in Figure 4a). The inner core occupies ∼45% of the radius of core and above the inner core is a liquid alloy that varies in composition by ∼1 wt % in sulfur content. The inflection in the contours of sulfur content in Figure 4a and the profile in Figure 4b at $R/R_c \sim 0.63$ is a consequence of the assumed linear melting curve as a function of sulfur content and the constant eutectic composition at pressures >7 GPa. The sloped

contours indicative of compositional stratification extend to the surface of the inner core in models with more realistic (though no better constrained at present) melting curves.

[20] The model run illustrated in Figure 4 is but one aspect of how the melting behavior of Fe-FeS could be manifested in the state of Ganymede's core. We can gain a fuller view by calculating how the boundaries between the possible core states (e.g., all liquid, Fe-snow and Fe-inner core, FeS floatation, etc.) vary as a function of temperature and composition. A representative example of these results is illustrated in Figure 5, which delineates these boundaries as a function of T_{cmb} and bulk core sulfur content for the situation where ice and rock mantle densities are the same as in Figure 4.

[21] There are eight possible core states outlined by these models. Each of the core states in Figure 5 labeled a−h is individually described below and has a corresponding schematic interpretation in Figures 6a−6h. The first state, a, is an entirely fluid core; temperatures throughout the core are higher than the melting temperature of the core alloy. Any convective motions in this regime must be generated purely thermally. Second state, b: for low sulfur contents the melting temperature of the core alloy increases with depth resulting in an Earth-like core structure with a mixed, fluid outer core and solid Fe inner core. Fluid motions may be generated by both thermal buoyancy and compositional buoyancy generated during crystallization of Fe at the ICB and the attendant release of light sulfur. Third state, c: at cooler CMB temperatures the solid Fe inner core is large enough that the sulfur content of the outer core has increased (because of conservation of sulfur) to the point where the melting temperature of the outer core starts decreasing with depth resulting in a core with both a stratified outer core due to Fe-snow (illustrated by the
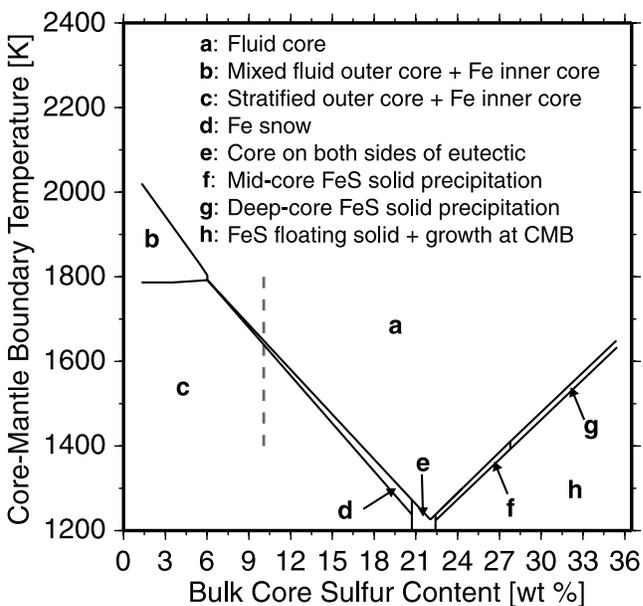

Figure 5. Phase stability zones as a function of core-mantle boundary temperature and bulk core sulfur content. Vertical dashed line indicates location of results presented in Figure 4a. See text for detailed explanations and Figure 6 for a schematic of each phase stability zone.
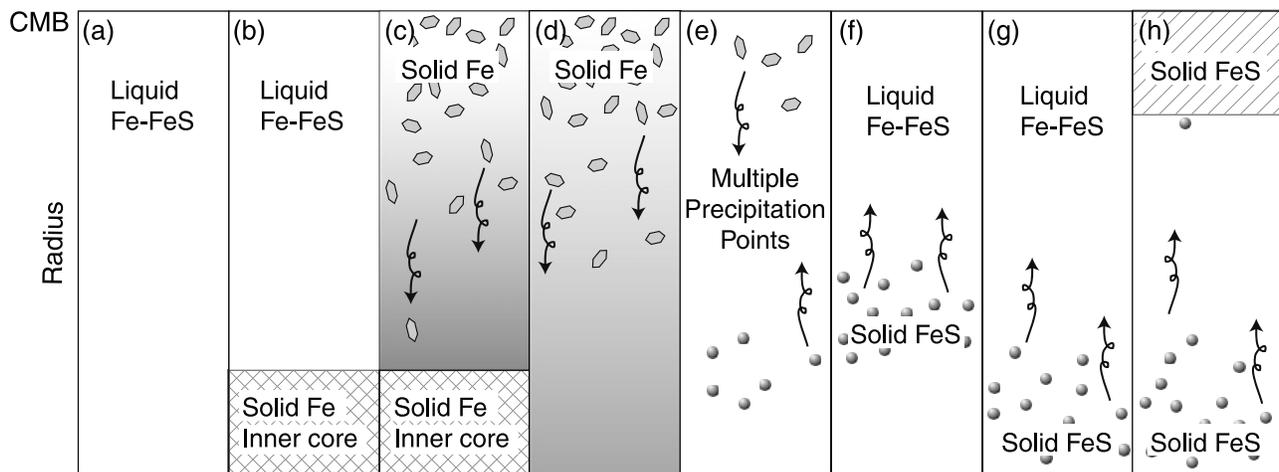
Figure 6. Schematic diagram of the eight potential core states for an Fe-FeS composition for Ganymede's core. Each panel (a–h) directly corresponds to the same modes (a–h) in Figure 5 and is explicitly described in the text. (a) Completely molten core. (b) An Earth-like core with a homogeneous outer core and solid Fe inner core. (c) A compositionally stratified outer core due to the shallow formation of Fe-snow and a solid Fe inner core. (d) Shallow precipitation of Fe-snow. (e) Multiple potential precipitation points due to bulk core composition that is either more Fe-rich or FeS-rich than eutectic as a function of depth. (g) Deep precipitation and floatation of solid FeS. (h) Deep precipitation and floatation of solid FeS and growth of a solid FeS layer at the CMB.

gradient shading in Figure 6c) and a solid Fe inner core. Motions in the liquid outer core can be generated thermally and by the inward segregation of iron from the Fe-snow and release of sulfur at the ICB. Fourth state, d: for high enough bulk core sulfur contents (>6 wt % S here), shallow Fe-snow precipitation can occur without the concurrent presence of an inner core (e.g., Figure 6d). The Fe-snow migrates deeper into the core because of its higher density, generating fluid motions along the way, and then remelts creating a higher iron content deep molten core. Further cooling eventually results in deep inner core growth due to the higher iron content and consequent higher melting temperatures there, and thus passage into state c. This pathway to from core states a to d to c is observed explicitly in Figure 4.

[22] In state e, because of the decrease in the sulfur content of the eutectic point with increasing pressure, up to 7 GPa, it is possible that for a given bulk composition that depending upon pressure (radial position) that the core may be both more Fe-rich and FeS-rich than eutectic. This region is small, covering a range of ~2 wt % bulk core sulfur content. The evolution of the precipitation of solids in this region is complex and not directly modeled here, only the boundaries are outlined. However, the first precipitates likely set the path of subsequent evolution. Formation of Fe-snow and subsequent deep sequestration of Fe will lead to lower local sulfur contents deep in the core pushing the compositions there back over to the Fe-rich side of the eutectic. A similar process pertains to FeS floatation, which will increase the shallow sulfur content leading to compositions on the FeS-rich side of the eutectic throughout the core.

[23] On the FeS-rich side of the eutectic (>22.5 wt % S in Figure 5) solidification and accumulation of FeS drives evolution of the core as it cools. Because of the high sulfur content of FeS (~36.5 wt % S) it is less dense than the residual liquid, resulting in dynamics that are different from the Fe-rich side. Starting from a completely molten core, as the system cools it first reaches a region where formation of FeS is favorable, either (state f) at midcore depths (at ~7 GPa) or (state g) deep near the center of the core where it floats upward and remelts before reaching the CMB (e.g., Figures 6f–6g). Midcore precipitation (state f) of FeS occurs due to the decrease in eutectic composition sulfur contents only up to 7 GPa (and remain constant at higher pressures) while eutectic melting temperatures continue to decrease with increasing pressure resulting in a local maxima in melting temperature at near-eutectic compositions. In state h, at cooler temperatures, the previous floatation and remelting of FeS has increased the sulfur content near the CMB enough to raise the melting point of the liquid such that solid FeS is stable near the CMB resulting in the process of precipitation of FeS both deep and near the CMB (e.g., Figure 6h).

[24] The broad structure of Figure 5 follows the assumed phase diagram for the core, but is modified by the existence of unique states such as Fe-snow (state d) and FeS floatation (states f and g). These two states occur over a relatively small temperature range suggesting that their influence (if any) on the evolution of Ganymede's core may be short-lived. Conditions of Fe-snow coupled with precipitation and growth of an inner core (state c) or FeS-floatation coupled with a solid outer core layer near the CMB (state h) extend over a much wider temperature range. It should be noted that the solid precipitation regimes on the FeS-rich side of the eutectic (states g and h) are not unique to Ganymede-like bodies, but are relevant to any modestly large body with an Fe-FeS core with higher than eutectic sulfur composition. However, the existence of additional solid phases at above 14 GPa [*Fei*

et al., 1997, 2000] may limit the FeS floatation regime for bodies with considerably higher pressure cores.

[25] The most interesting aspect of Figure 5 is the relatively small extent of the Earth-like regime (labeled b). Indeed, with cool enough CMB temperatures it appears that shallow formation of Fe-snow in the presence of a deep, solid Fe inner core (labeled c) is the most likely state on the Fe-rich side of the eutectic. The results presented in Figure 5 are quite general. There are only minor differences between

the boundaries for various core states for different internal structures, due in large part to the fact that the range of core pressures does not vary drastically among the different internal structure models.

3.2. Thermochemical Core Evolution

[26] In order to understand how Ganymede's core might evolve and which core states are likely at the present-day, we modeled the coupled internal thermal evolution of the satellite's rock mantle and the thermochemical evolution of the metallic core. Thermal evolution models were restricted to the Fe-rich side of the eutectic composition for the sake of simplicity; a choice that is also in step with the low sulfur content of ordinary chondrites inferred to be consistent with Ganymede's internal structure [*Kuskov and Kronrod*, 2001]. A focused set of calculations were performed to determine how the satellite's core might evolve to or through some of the solid precipitation regimes on the Fe-rich side of the eutectic in Figure 5. Figure 7 illustrates typical thermal evolution calculations over 4.5 Gyr for three models that encompass a factor of four variation in rock mantle heat production (i.e., one-half to twice CI chondritic), yet retain the same internal structure (the star on Figure 1 with a bulk core sulfur content of 10 wt %). The model cases in Figure 7 demonstrate three possible temporal evolutions of Ganymede's interior for the same structure and core composition indicated by the vertical dashed line in Figure 5. Temperatures (Figure 7a) at the CMB show a rapid decrease from the starting temperature of 2000 K down to a value near 1900 K consistent with and adiabatic temperature gradient throughout the mantle. Mantle and CMB temperatures over time generally parallel the decrease in heat output from radiogenic elements as they decay; the absolute offsets between the models, e.g., the ~150 K difference between one-half and twice CI chondritic models after 4.5 Gyr, reflects the total amount of heat production. Figure 7a demonstrates the modest effects of varying initial conditions on primary model results; there is an ~0.5 Gyr period of adjustment of core and mantle temperatures followed by a decline that follows the decay of radiogenic heat production and the results for the core state after several Gyr are relatively insensitive to initial conditions, consistent with previous work [i.e., *Hauck et al.*, 2004]. The small kinks in the CMB temperature profiles for the chondritic and one-half chondritic cases are due to the increased heat output from the core (Figure 7b) resulting from the latent heat and
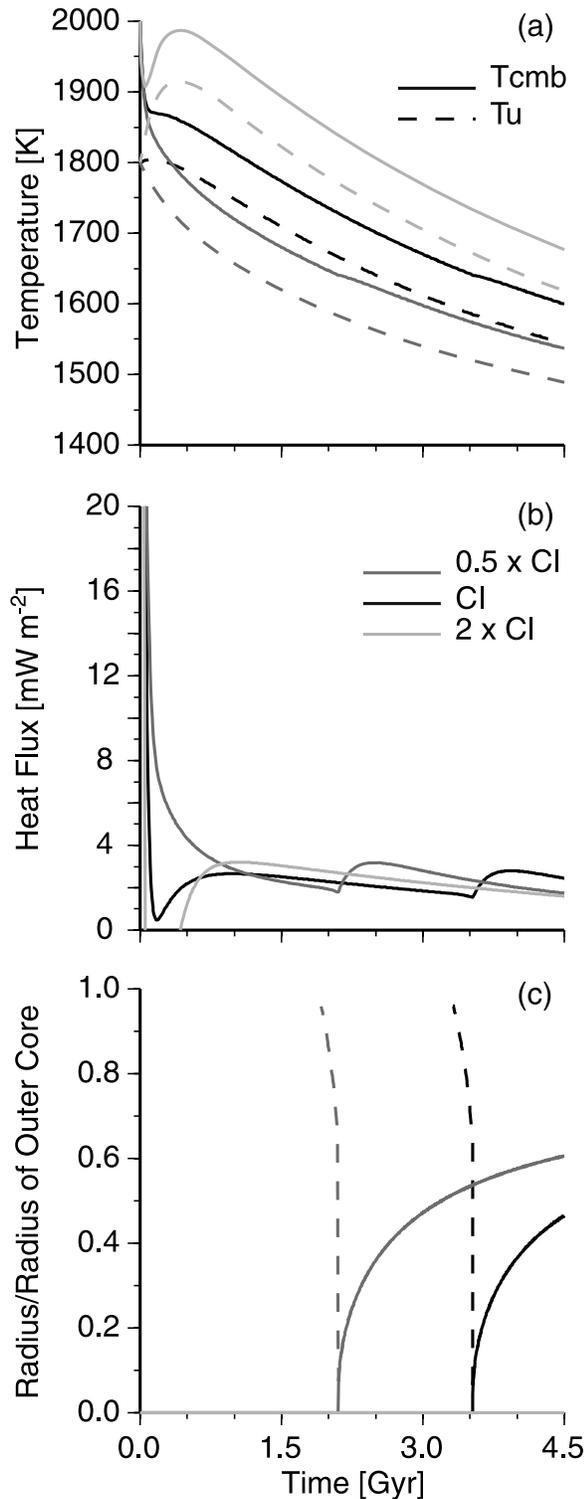

Figure 7. Results illustrating three examples of thermal evolution models for a model structure with 10 wt % bulk core sulfur content (the star in Figure 1) and varying amounts of heat production over 4.5 Gyr. Legend for heat production for all three panels is shown in (b). (a) Temperatures at the CMB (T_{cmb}) and the base of the thermal lithosphere (T_u). (b) Heat flux out of the core at the CMB (q_c). (c) Precipitation boundaries within the core. Dashed lines indicate the boundary above which Fe-snow is formed; regions below the dashed lines at a given time are entirely liquid. Solid lines indicate the location of the inner core boundary (ICB). The core is solid below the line, and the core is liquid, but Fe-snow formation is favorable, above the line.
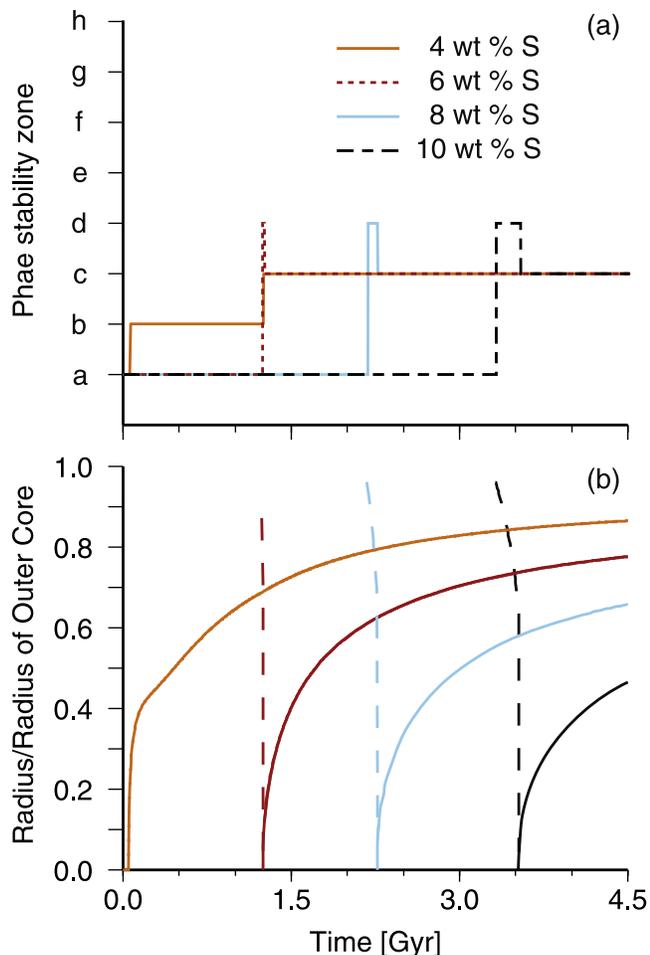
Figure 8. State of the core as a function of time. (a) Evolution of the core state for four bulk core sulfur contents and CI chondritic heat production. Phase stability zone labels correlate with Figures 5 and 6. Model with 4 wt % sulfur passes through period with an Earth-like core evolution prior to beginning precipitation of Fe-snow. (b) Precipitation boundaries within the core. See also Figure 7c for additional details.

gravitational energy released during inner core growth (Figure 7c). The interval over which Fe-snow is the sole precipitation mechanism in these model cases is short, ~200 Myr as determined from the dashed line in Figure 7c. Figure 8 illustrates the time evolution of the state of the core for four model cases with varying sulfur content and CI chondritic heat production in the rock mantle. The length of time periods where precipitation of solid Fe in the absence of an inner core is relatively limited, at most a few hundred Myr in all the models presented. These results generally hold for the one-half and twice chondritic models as well due to the identical rates of parent radioisotope loss (see the dashed lines in Figure 7c for comparison). The core state models and the results in Figure 8 suggest that the existence and size of the inner core is a useful, if not unique, indicator of the physical state of the core.

[27] We calculated potential thermal evolution scenarios for six suites of models to characterize the effects of variations in satellite internal structure and heat production

on core evolution as a function of the sulfur content of the core alloy. Results from internal evolution model runs after 4.5 Gyr for normalized inner core radius as a function of sulfur content of the core are presented in Figure 9. These results focus on two parameters that may affect evolution of the core: (1) variation of internal structure (e.g., densities and hence thicknesses of ice and rock) and (2) variation in the amount of heat produced by natural decay of radioactive elements in the rock mantle. At low bulk core sulfur contents all of the models converge toward the point where a pure Fe core would be completely solid at present because each model has a T_{cmb} less than the pure Fe melting temperature. Variations in the densities of the ice and silicate layers do not lead to considerable differences in time-integrated core evolution; even the difference between the maximum sulfur content for the existence of an inner core is less than 2 wt %, which is the maximum difference between the four suites of models with differing internal structures. This result suggests that thermal history models for Ganymede's core are robust regardless of the uncertainty on the internal structure of the satellite.

[28] The effects of silicate mantle heat productivity on core evolution are more pronounced than those due to the internal structure. The composition of heat-producing elements in Ganymede is unconstrained; therefore we calculate thermal evolution models for a wide range of possible heat-productivities. A variation in total heat-producer concentration of a factor of four results in a range of ~4 wt % maximum bulk core sulfur content for models that contain an inner core at present. Predictably, the suite of model cases with the higher concentration of heat-producing elements has smaller inner core sizes, for a given core sulfur content, than those with lower concentrations because
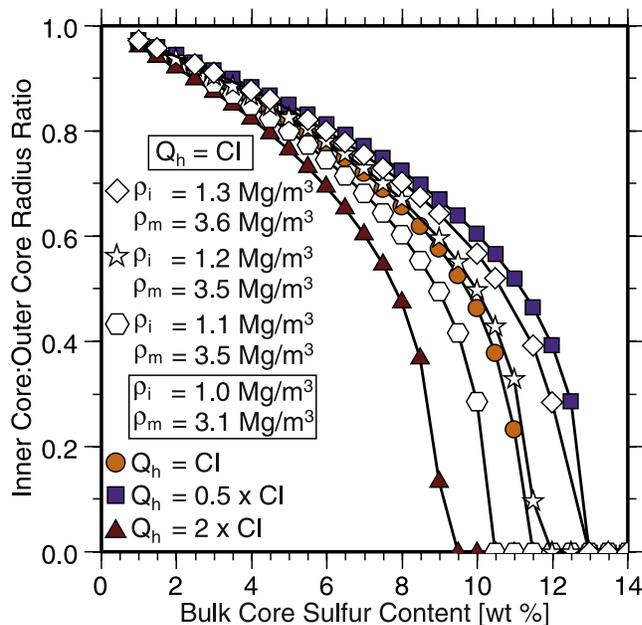

Figure 9. Present-day inner core:outer core radius ratio as a function of bulk core sulfur content for models with varying internal structures (open symbols and solid circle) with the same internal heat production and varying amounts of heat production (solid symbols).

the cores cool more slowly. The larger mantle heat-production results in higher CMB temperatures throughout history, limiting the amount of inner core growth.

[29] An interesting result from these evolution models is that all of the runs with inner cores after 4.5 Gyr also have Fe-snow conditions at shallow levels. Each of the models with inner cores has cooled through the Earth-like or Fe-snow, respectively (Figure 5, regimes b and d). Core convection requires a thermal or compositional buoyancy source. Heat flux out of the core in these models after 4.5 Gyr of evolution range from $\sim$1 to 3.3 mW m^{-2}. A requirement for a thermally driven dynamo is that the heat flux out of the core must exceed that which can be conducted along the adiabat at the core-mantle boundary [e.g., *Merrill et al.*, 1998]. Assuming a core thermal conductivity of 40 W m K^{-1} [e.g., *Stacey and Anderson*, 2001], only models with twice chondritic heat production and $\sim$6–8.5 wt % bulk core sulfur content satisfy this dynamo requirement after 4.5 Gyr. The implication is that mixing due to compositional buoyancy is likely important for driving convection in Ganymede's core, a condition satisfied by models with solid Fe or FeS precipitation in any of the modes (b–h) in Figures 5 and 6.

4. Magnetic Field Scaling Estimates

[30] The presence of an internally generated magnetic field within Ganymede is likely indicative of active internal processes [e.g., *Kivelson et al.*, 2002]. The overlap between laboratory experimental conditions and the pressures and temperatures that prevail in Ganymede's core provides an important window into core processes, free of extrapolation to higher pressures. Ganymede presents an opportunity to investigate thermodynamic aspects of the process with available data on potential core materials [*Fei et al.*, 1997, 2000]. The iron snow process is the result of the decrease in eutectic melting temperature with pressure up to $\sim$14 GPa in the Fe-FeS system [*Fei et al.*, 1997]. While sulfur is not the only candidate light alloying element for metallic cores, it is consistent with the high volatile content of icy satellites like Ganymede, the presence of iron sulfides in meteorites, the abundance of sulfur at Io [e.g., *Lewis*, 1982], and recent models that suggest a composition similar to L or LL chondrites [*Kuskov and Kronrod*, 2001].

[31] Generation of a magnetic field by core dynamo action requires the presence of motions within the liquid portion of Ganymede's metallic core. These motions are likely not driven by purely thermal buoyancy because the present-day heat flux out of the core in most of scenarios investigated is at least marginally less than the $\sim$1.5–4 mW/m^2 that can be conductively transported along an adiabat. In the absence of significant heat production in the core, convection driven by compositional buoyancy forces related to the separation of solid precipitates from the liquid core is the most likely driver of the dynamo. In larger bodies like the Earth, compositional convection can manifest itself through the growth of the inner core and consequent expulsion of the light constituent, which buoyantly rises through and mixes the outer core. In the case of Ganymede, however, Fe-snow may settle inward (or solid FeS may float outward) through the outer core causing mixing. The Fe-snow process establishes a stable compo-

sitional gradient; however, even with a stable compositional gradient and an inner core, there is still a net transfer of Fe inward as the result of continued cooling and precipitation of solid Fe.

[32] Thus far, we have assumed that the presence of a compositional buoyancy source alone will drive convection and generate a magnetic field at Ganymede. The presence of a buoyancy source is a necessary condition, but may not be sufficient to drive a dynamo. Using the results of recent laboratory and numerical experiments [*Aubert et al.*, 2001; *Aurnou et al.*, 2003; *Aubert*, 2005] and those presented here we can make simple estimates of the Rossby number, Ro (the ratio of inertial to Coriolis forces [*Tritton*, 1988]), and the magnetic Reynolds parameter, Re_m (the ratio of magnetic induction to magnetic diffusion), both of which are crucial parameters for assessing the likelihood of dynamo action.

[33] The Rossby and magnetic Reynolds numbers both depend directly on the typical flow velocity, U, in the fluid portion of the core. Laboratory experiments [*Aurnou et al.*, 2003] and numerical dynamo simulations [*Aubert*, 2005] indicate that typical zonal flow velocities scale with the buoyancy flux, F, as

$$U \sim \left(\frac{F}{\Omega}\right)^{1/2}, \qquad (7)$$

where

$$F \simeq \left(\frac{\Delta\rho}{\rho_c}\right) g_{cmb} \frac{dR_{ic}}{dt}, \qquad (8)$$

and $\Omega = 1 \times 10^{-5}$ s^{-1} is Ganymede's angular rate of rotation. The buoyancy flux depends on the local gravity where buoyancy is generated, which is near the CMB for iron snow ($g_{cmb} \approx 1$ m s^{-2}). The density contrast between the liquid and solid is taken to be $\Delta\rho \sim 1000$ kg m^{-3} by analogy with the density contrast across Earth's ICB [*Gubbins et al.*, 2004] and we take the mean core density to be $\rho_c = 5990$ kg m^{-3} corresponding to our model with 10 wt % S (see white star in Figure 1 and Figure 4). For the iron snow regime, the value of F is related to the inner core growth rate since solid Fe, which forms at the CMB, eventually accumulates on the ICB after falling through the fluid outer core. The inner core growth rate after 4.5 Gyr from the thermal evolution model (solid circle at 10 wt % S in Figure 9) is $dR_{ic}/dt = 3 \times 10^{-12}$ m s^{-1} and which results in a buoyancy flux of $F \approx 5 \times 10^{-13}$ m^2 s^{-3} and flow velocities of $U \approx 0.2$ mm s^{-1}. We refer to this model case as "Fe-snow-IC." Other models for the evolution of the core have faster (slower) rates of solid formation, roughly associated with smaller (larger) inner core sizes, but these values are of the appropriate order of magnitude and the flow velocities are less sensitive to these rates because $U \sim F^{1/2}$. This flow velocity allows us to determine the Rossby number, $Ro = U/(2\Omega R_{cmb}) \approx 10^{-5}$, and magnetic the Reynolds number, $Re_m = (U R_{cmb})/\eta \approx 10^2$ for an assumed magnetic diffusivity, $\eta = 2$ m^2 s^{-1}. These results with Ro much less than unity and Re_m approaching $O(10^2)$ are both consistent with Ganymede's magnetic field plausibly being generated by dynamo action in the core [e.g., *Gubbins and*

Roberts, 1987; *Jones*, 2000; *Christensen and Aubert*, 2006].

[34] We can extend this line of reasoning to the case "Fe-snow-no-IC" of a core in the Fe-snow only regime (i.e., with no inner core). This corresponds to case d in Figures 5 and 6, where the buoyancy flux is generated below the CMB. In this situation in which no inner core exists, we estimate the buoyancy flux in terms of the change in composition, and via the density of the residual liquid using

$$F \simeq \frac{g_{cmb}R_c}{\rho_c}\frac{d\chi_s}{dt}\frac{d\rho}{d\chi_s} \tag{9}$$

in place of equation (8) where $d\chi_s/dt$ is the change in sulfur content with time evaluated at the CMB and $d\rho/d\chi_s$ is an estimate of the change in density with sulfur content at Ganymede's CMB pressures based upon our structural models (e.g., Figure 1) of $\sim$90 kg m^{-3} per 1 wt % sulfur. Though results vary with time, for the same thermal evolution model used in the previous case, Fe-snow-IC that has an inner core, the buoyancy flux averaged over the $\sim$200 Myr period of Fe-snow formation without an inner core (e.g., Figure 8a) is $F \approx 1 \times 10^{-11}$ m^2 s^{-3}. This buoyancy flux for the Fe-snow-no-IC case is a factor of 20 greater than for the Fe-snow-IC case, which results in Rossby and magnetic Reynolds parameters $20^{1/2} \approx 4.5$ times greater. These increased values are also both consistent with dynamo action in the core.

[35] Recent numerical dynamo studies provide empirical scaling laws for planetary dynamo magnetic field strength, B, as a function of the dynamo simulation control parameters [*Christensen and Aubert*, 2006; *Olson and Christensen*, 2006]. Both these studies find that dipole-dominated magnetic fields can be produced in a regime in which B scales with the buoyancy flux, F, and is largely independent of planetary rotation rate and electrical conductivity. This result is surprising as it has long been supposed that planetary magnetic field strength scales with planetary rotation rate (see *Stevenson* [2003] for a recent review). For small Ro and $Re_m > \sim$50, *Christensen and Aubert* [2006] provide the following empirical scaling law for volumetrically averaged magnetic field strength as a function of buoyancy flux:

$$B \approx \mu_o^{1/2}\rho_c^{1/2}\left(\frac{R_{ic}FD}{R_c}\right)^{1/3}, \tag{10}$$

where the permeability of free space, μ_0 is $4\pi \times 10^{-7}$ H m^{-1}, D is the thickness of the outer core, and the other parameters have been previously defined. The estimates for the Rossby and magnetic Reynolds parameters for the iron-snow regimes are consistent with the assumptions of this recent empirical scaling law; hence we are justified in calculating order-of-magnitude estimates of magnetic field strength for our example cases with iron-snow driven fluid motions. For the Fe-snow-IC case (iron-snow with a growing inner core), $R_c/R_p \approx 0.25$ and $R_i/R_c \approx 0.45$ at present, which results in a volumetrically averaged magnetic field strength in the core of $B \approx 3.8 \times 10^5$ nT. However, many numerical models find that the magnetic field at core-mantle boundary is roughly an order of magnitude less than the volume averaged core field [e.g.,

Heimpel et al., 2005]. With a factor of 10 reduction in magnitude volumetrically averaged field strength at the surface of the core and the fact that the dipolar component of the field will geometrically attenuate as $(R_c/R_p)^3$, the predicted surface value of B is $\sim$600 nT. This magnetic field estimate is in good basic agreement with the observed value of Ganymede's equatorial surface field of $\sim$750 nT [*Kivelson et al.*, 2002].

[36] The magnetic field scaling estimate for Fe-snow-no-IC case (Fe-snow only regime with no inner core) is similar to the Fe-snow-IC case. For this model, which has no inner core but a larger compositional buoyancy flux, we follow the arguments of *Christensen and Aubert* [2006] for their estimate of Jupiter's magnetic field intensity; we consider an appropriate effective length scale for the potentially distributed buoyancy production to be $R_c/2$ and hence replace both D and R_{ic} in equation (10) with $R_c/2$. This leads to a magnetic field strength estimate of $B \approx 1600$ nT early on in Ganymede's thermal evolution, when the Fe-snow-no-IC case is applicable. Thus our B estimates, which are based on state-of-the-art numerical dynamo scaling laws, demonstrate that the buoyancy fluxes inferred for the Fe-snow regime are potentially capable of generating planetary magnetic fields that are comparable to those observed on Ganymede.

5. Discussion

[37] Compositional buoyancy driven convective motions in Ganymede's core are possible when a solid is precipitated. If solid precipitation is required for the dynamo, then it may be possible to place bounds on the amount of sulfur in the core. For example, on the Fe-rich side of the Fe-FeS eutectic, we might find a maximum sulfur content and on the FeS-rich side a minimum. However, maximum sulfur contents based on Figure 9 cannot be taken at face value because of the lack of data on the compositional dependence of the liquidus at high pressures. A preliminary study utilized a liquidus with a nonlinear dependence on mass fraction of sulfur [*Hauck et al.*, 2002], but given the lack of relevant experimental data, this added unconstrained complexity, though plausible, is not justified. The simple, linear liquidus employed here is more sophisticated than typical implementations because of the pressure dependence of equation (4). However, it underpredicts, relative to a nonlinear liquidus, the melting temperature at all compositions except the Fe and FeS end-members and the eutectic point. Consequently, our results underpredict the CMB temperatures necessary for precipitation of solids relative to a more complex liquidus. Compared to our current approach, a nonlinear liquidus results in a shift to higher CMB temperatures and to larger sulfur contents (by a few wt %) being required to achieve similar amounts of solid precipitation and thus a higher maximum sulfur content on the Fe-rich side of the eutectic than calculated above (cf. Figure 9). None of the major conclusions are affected by the linear liquidus. Fe-snow and FeS floatation are possible, and concurrent Fe-snow and solid Fe inner core growth are favored at present for models with sulfur contents less than the eutectic composition.

[38] The thermal evolution scenarios that have been explored (Figure 9), though not exhaustive, illustrate a wide

range of possibilities, especially with respect to the importance of internal heat production in the rock mantle. The assumption that the mantle convects in the stagnant-lid regime is a reasonable starting point because the majority of solid planets with mantle convection, save Earth, do so with stagnant lids. Implementation of a wet rheology is consistent with Ganymede's water-rich composition. However, though a sub-ice plate tectonic regime cannot be ruled out a priori and would likely result in stronger cooling of the core and hence greater ease in driving convective motions, such a notion at present is speculative at best.

[39] Coupled orbital-thermal evolution models [*Showman et al.*, 1997] suggest that if Ganymede passed through a resonance, tidal heating events would have warmed the interior and potentially resurfaced the satellite. Such events, if they occurred, would be additional sources of heat in the interior that are not accounted for in our models. However, beyond the possible link between such a reheating event and the formation of grooved terrain, potentially in the last billion years [e.g., *Showman et al.*, 1997], it is not possible to reasonably constrain the total amount of tidal dissipation (and hence heating) that might have occurred within the silicate mantle. *Zahnle et al.* [2003] speculated that a thermal cooling timescale of ∼1 Gyr is an upper bound to the age of Ganymede's dynamo and that cooling would commence at the end of nonsynchronous rotation for the satellite. Such a timescale provides an avenue to estimate absolute cratering rates. However, compositional buoyancy (any of the regimes in Figures 5 and 6 except for the case of an entirely molten core) can generate fluid motions over much longer timescales, rendering an absolute timing relationship between the origin of Ganymede's dynamo and the end of nonsynchronous rotation ambiguous. More to the point, tidal heating could only delay solid precipitation, not prevent it. Hence the effects of tidal heating should not fundamentally alter our conclusion that shallow Fe-snow precipitation is an inevitable consequence of cooling of Ganymede's core for core compositions more Fe-rich than eutectic.

6. Summary and Conclusions

[40] Ganymede presents a unique opportunity to investigate the driving forces behind dynamo generation for a body where we have unprecedented, unextrapolated information about potential core-forming materials. Furthermore, the melting behavior of Fe-FeS alloys that may be present in the core of Jupiter's largest moon suggest that a potentially novel set of mechanisms may drive convective motions in the satellite's core, e.g., Fe-snow and FeS floatation. We demonstrate that indeed these mechanisms are likely; Fe-snow will tend to form on the Fe-rich side of the eutectic, while FeS-floatation will occur on the FeS-rich side. In fact, these processes are an inevitable consequence of cooling an Fe-FeS core in a body similar in size to Ganymede. Furthermore, thermal evolution models of cores on the Fe-rich side of the eutectic suggest that convection driven by compositional buoyancy released during concurrent shallow Fe-snow formation and deep inner core growth is a potentially significant driver of Ganymede's present-day magnetic field. New developments in our understanding of Ganymede's magnetic field will likely derive from improved knowledge of the melting relationships of core forming materials (e.g., Fe-FeS alloys) and dynamo modeling in the presence of modest compositional gradients.

References

Anderson, J. D., E. L. Lau, W. L. Sjogren, G. Schubert, and W. B. Moore (1996), Gravitational constraints on the internal structure of Ganymede, *Nature*, *384*, 541–545.

Anderson, O. L. (2003), The three-dimensional phase diagram of iron, in *Earth's Core: Dynamics, Structure, Rotation*, Geodyn. Ser., vol. 31, edited by V. Dehant et al., pp. 83–103, AGU, Washington, D. C.

Anderson, W. W., and T. J. Ahrens (1994), An equation of state for liquid iron and implications for the Earth's core, *J. Geophys. Res.*, *99*, 4273–4284.

Aubert, J. (2005), Steady zonal flows in spherical shell dynamos, *J. Fluid Mech.*, *542*, 53–76.

Aubert, J., D. Brito, H. C. Nataf, P. Cardin, and J. P. Masson (2001), A systematic experimental study of spherical shell convection in water and liquid gallium, *Phys. Earth Planet. Inter.*, *128*, 51–74.

Aurnou, J., S. Andreadis, L. Zhu, and P. Olson (2003), Experiments on convection in Earth's tangent cylinder, *Earth Planet. Sci. Lett.*, *221*, 119–134.

Balog, P. S., R. A. Secco, D. C. Rubie, and D. J. Frost (2003), Equation of state of liquid Fe-10 wt % S: Implications for the metallic cores of planetary bodies, *J. Geophys. Res.*, *108*(B2), 2124, doi:10.1029/2001JB001646.

Boehler, R. (1992), Melting of the Fe-FeO and the Fe-FeS systems at high pressure: Constraints on core temperatures, *Earth Planet. Sci. Lett.*, *111*, 217–227.

Boehler, R. (1996), Melting of mantle and core materials at very high pressures, *Phil. Trans. R. Soc. London, Ser. A*, *354*, 1265–1278.

Brownlow, A. H. (1996), *Geochemistry*, 580 pp., Simon and Schuster, Upper Saddle River, N. J.

Buffett, B. A., H. E. Huppert, J. R. Lister, and A. W. Woods (1996), On the thermal evolution of the Earth's core, *J. Geophys. Res.*, *101*, 7989–8006.

Christensen, U. R., and J. Aubert (2006), Scaling properties of convection-driven dynamos in rotating spherical shells and application to planetary magnetic fields, *Geophys. J. Int.*, *166*, 97–144.

Crary, F. J., and F. Bagenal (1998), Remanent ferromagnetism and the interior structure of Ganymede, *J. Geophys. Res.*, *103*, 25,757–25,774.

Fei, Y., C. T. Prewitt, H. K. Mao, and C. M. Bertka (1995), Structure and density of FeS at high pressure and high temperature and the internal structure of Mars, *Science*, *268*, 1892–1894.

Fei, Y., C. M. Bertka, and L. W. Finger (1997), High-pressure iron sulfur compound, Fe_3S_2, and melting relations in the Fe-FeS system, *Science*, *275*, 1621–1623.

Fei, Y., J. Li, C. M. Bertka, and C. T. Prewitt (2000), Structure type and bulk modulus of Fe_3S, a new iron-sulfur compound, *Am. Mineral.*, *85*, 1830–1833.

Gubbins, D. (1977), Energetics of the Earth's core, *J. Geophys.*, *43*, 453–464.

Gubbins, D., and P. H. Roberts (1987), Magnetohydrodynamics of the Earth's core, in *Geomagnetism*, edited by J. A. Jacobs, pp. 1–183, Elsevier, New York.

Gubbins, D., D. Alfè, G. Masters, G. D. Price, and M. J. Gillan (2004), Gross thermodyamics of two-component core convection, *Geophys. J. Int.*, *157*, 1407–1414.

Hauck, S. A., II, and R. J. Phillips (2002), Thermal and crustal evolution of Mars, *J. Geophys. Res.*, *107*(E7), 5052, doi:10.1029/2001JE001801.

Hauck, S. A., II, A. J. Dombard, S. C. Solomon, and J. M. Aurnou (2002), Internal structure and mechanisms of core convection on Ganymede, *Lunar Planet. Sci.* [CD-ROM], *XXXIII*, abstract 1380.

Hauck, S. A., II, A. J. Dombard, R. J. Phillips, and S. C. Solomon (2004), Internal and tectonic evolution of Mercury, *Earth Planet. Sci. Lett.*, *222*, 713–728.

Heimpel, M. H., J. M. Aurnou, F. M. Al-shamali, and N. Gomez-Perez (2005), A numerical study of dynamo action as a function of spherical shell geometry, *Earth Planet. Sci. Lett.*, *236*, 542–557.

Hillgren, V. J., C. K. Gessmann, and J. Li (2000), An experimental perspective on the light element in the Earth's core, in *Origin of the Earth*

and Moon, edited by R. M. Canup, and K. Righter, pp. 245–263, Univ. of Arizona Press, Tucson.

Jones, C. A. (2000), Convection-driven geodynamo models, *Phil. Trans. R. Soc. London, Ser. A*, *358*, 873–897.

Karato, S.-I., and P. Wu (1993), Rheology of the upper mantle: A synthesis, *Science*, *260*, 771–778.

Kirk, R. L., and D. J. Stevenson (1987), Thermal evolution of a differentiated Ganymede and implications for surface features, *Icarus*, *69*, 91–134.

Kivelson, M. G., K. K. Khurana, C. T. Russell, R. J. Walker, J. Warnecke, F. V. Coroniti, C. Polanskey, D. J. Southwood, and G. Schubert (1996), Discovery of Ganymede's magnetic field by the Galileo spacecraft, *Nature*, *384*, 537–541.

Kivelson, M. G., K. K. Khurana, and M. Volwerk (2002), The permanent and inductive magnetic moments of Ganymede, *Icarus*, *157*, 507–522.

Kuang, Z., and D. J. Stevenson (1996), Magnetic field generation in the Galilean satellites, *Eos Trans. AGU*, *77*(46), Fall Meet. Suppl., F437.

Kuskov, O. L., and V. A. Kronrod (2001), Core sizes and internal structure of Earth's and Jupiter's satellites, *Icarus*, *151*, 204–227.

Labrosse, S. (2003), Thermal and magnetic evolution of the Earth's core, *Phys. Earth Planet. Inter.*, *140*, 127–143.

Labrosse, S., J.-P. Poirier, and J.-L. Le Mouël (2001), The age of the inner core, *Earth Planet. Sci. Lett.*, *190*, 111–123.

Lewis, J. S. (1982), Io: Geochemistry of sulfur, *Icarus*, *50*, 103–114.

Loper, D. E. (1978), The gravitationally powered dynamo, *Geophys. J. R. Astron. Soc.*, *54*, 389–404.

Loper, D. E., and P. H. Roberts (1979), Are planetary dynamos driven by gravitational settling?, in *Origins of Planetary Magnetism*, edited by L. J. Srnka and R. B. Merrill, pp. 192–193, Elsevier, New York.

Loper, D. E., and P. H. Roberts (1983), Compositional convection and the gravitationally powered dynamo, in *Stellar and Planetary Magnetism*, edited by A. M. Soward, pp. 297–327, Gordon and Breach, New York.

McKinnon, W. B. (1996), Core evolution in the icy Galilean satellites, and the prospects for dynamo-generated magnetic fields, *Bull. Am. Astron. Soc.*, *28*, 1076.

Merrill, R. T., M. W. McElhinny, and P. L. McFadden (1998), *The Magnetic Field of The Earth*, 531 pp., Elsevier, New York.

Murthy, V. R., and H. T. Hall (1970), The chemical composition of the Earth's core: Possibility of sulphur in the core, *Phys. Earth Planet. Inter.*, *2*, 276–282.

Olson, P. L., and U. R. Christensen (2006), Dipole moment scaling for convection-driven planetary dynamos, *Earth Planet. Sci. Lett.*, in press.

Palguta, J. L., J. D. Anderson, G. Schubert, and W. B. Moore (2006), Mass anomalies on Ganymede, *Icarus*, *180*, 428–441.

Poirier, J. P. (2000), *Introduction to the Physics of the Earth's Interior*, 312 pp., Cambridge Univ. Press, New York.

Ranalli, G. (1995), *Rheology of the Earth*, 413 pp., CRC Press, Boca Raton, Fla.

Sanloup, C., F. Guyot, P. Gillet, G. Fiquet, M. Mezaouar, and I. Martinez (2000), Density measurements of liquid Fe-S alloys at high-pressure, *Geophys. Res. Lett.*, *27*, 811–814.

Schubert, G., M. N. Ross, D. J. Stevenson, and T. Spohn (1988), Mercury's thermal history and the generation of its magnetic field, in *Mercury*, edited by F. Vilas, C. R. Chapman, and M. S. Matthews, pp. 429–460, Univ. of Arizona Press, Tucson.

Schubert, G., K. Zhang, M. G. Kivelson, and J. D. Anderson (1996), The magnetic field and internal structure of Ganymede, *Nature*, *384*, 544–545.

Schubert, G., D. L. Turcotte, and P. Olson (2001), *Mantle Convection in the Earth and Planets*, 940 pp., Cambridge Univ. Press, New York.

Schubert, G., J. D. Anderson, T. Spohn, and W. B. McKinnon (2004), Interior composition, structure and dynamics of the Galilean satellites, in *Jupiter: The Planet, Satellites, and Magnetosphere*, edited by F. Bagenal, T. Dowling, and W. B. McKinnon, pp. 281–306, Cambridge Univ. Press, New York.

Scott, H. P., Q. Williams, and F. J. Ryerson (2002), Experimental constraints on the chemical evolution of large icy satellites, *Earth Planet. Sci. Lett.*, *203*, 399–412.

Showman, A. P., D. J. Stevenson, and R. Malhotra (1997), Coupled orbital and thermal evolution of Ganymede, *Icarus*, *129*, 367–383.

Solomatov, V. S. (1995), Scaling of temperature and stress-dependent viscosity convection, *Phys. Fluids*, *7*, 266–274.

Solomatov, V. S., and L.-N. Moresi (2000), Scaling of time-dependent stagnant-lid convection: Application to small-scale convection on Earth and other terrestrial planets, *J. Geophys. Res.*, *105*, 21,795–21,817.

Stacey, F. D., and O. L. Anderson (2001), Electrical and thermal conductivities of Fe-Ni-Si alloy under core conditions, *Phys. Earth Planet. Inter.*, *124*, 153–162.

Stevenson, D. J. (2003), Planetary magnetic fields, *Earth Planet. Sci. Lett.*, *208*, 1–11.

Stevenson, D. J., T. Spohn, and G. Schubert (1983), Magnetism and thermal evolution of the terrestrial planets, *Icarus*, *54*, 466–489.

Tritton, D. J. (1988), *Physical Fluid Dynamics*, 544 pp., Oxford Univ. Press, New York.

Turcotte, D. L., and G. Schubert (1982), *Geodynamics*, 448 pp., John Wiley, Hoboken, N. J.

Usselman, T. M. (1975), Experimental approach to the state of the core; Part I, The liquidus relations of the Fe-rich portion of the Fe-Ni-S system from 30 to 100 kb, *Am. J. Sci.*, *275*, 278–290.

Zahnle, K., P. Schenk, H. Levison, and L. Dones (2003), Cratering rates in the outer solar system, *Icarus*, *163*, 263–289.

————————————

J. M. Aurnou, Department of Earth and Space Sciences, University of California at Los Angeles, Los Angeles, CA 90032, USA.

A. J. Dombard, Applied Physics Laboratory, Johns Hopkins University, Laurel, MD 20723, USA.

S. A. Hauck, II, Department of Geological Sciences, Case Western Reserve University, Cleveland, OH 44106-7216, USA. (hauck@case.edu)